Journal of Physics: Conference Series

Wolf-Rayet nebulae

To cite this article: You-Hua Chu 2016 *J. Phys.: Conf. Ser.* **728** 032007

Wolf-Rayet nebulae

You-Hua Chu[1]

[1] Institute of Astronomy and Astrophysics, Academia Sinica
AS/NTU, No.1, Sec. 4, Roosevelt Rd, Taipei 10617, Taiwan, R.O.C.

E-mail: [1] `yhchu@asiaa.sinica.edu.tw`

Abstract. Since the discovery of nebulae around Wolf-Rayet (WR) stars in the 1960s, it has been established that WR stars are massive stars at advanced evolutionary stages and that their surrounding nebulae result from the interactions between the stellar mass loss and the ambient interstellar medium. Surveys of WR nebulae have been made in the Galaxy, Magellanic Clouds, and other nearby galaxies in the Local Group. Some WR nebulae exhibit He II λ4686 line emission, indicating stellar effective temperatures of $90 - 100 \times 10^3$ K. The shocked fast stellar winds from WR nebulae have been detected in soft X-rays, but theoretical models have not been able to reproduce the observed X-ray spectral properties. Elemental abundances of WR nebulae consisting of synthesized stellar material can constrain stellar evolution models, but high-dispersion spectra are needed to kinematically separate the expanding shell of a WR nebula and the background interstellar medium for accurate abundance analyses.

1. Wolf-Rayet stars and their nebulae

The first three nebulae around Wolf-Rayet (WR) stars were reported in 1965 by Johnson and Hogg [1]: NGC2359, NGC6888, and S308. The ring-like morphology of these WR nebulae is indicative of a shell structure. It was immediately suggested that stellar outflows implied by the broad P Cygni line profiles were responsible for shaping the nebulae, although the evolutionary status of WR stars was not well known and the outflows were later called fast stellar winds.

Models of massive star evolution have been guided by observations, in particular, the distribution of massive stars in the Hertzsprung-Russel diagram (HRD) plotted in stellar effective temperature (T_{eff}) versus bolometric magnitude (M_{Bol}) by Humphreys and Davidson [2]. An absence of very luminous red stars in the HRD was observed, and this so-called Humphrey and Davidson Limit provided essential constraints to models of stellar evolution. It is now known that the most massive O stars, $\sim 60 M_{\odot}$ or higher, evolve off the main sequence to become luminous blue variables (LBVs), while the less massive O stars evolve into red supergiants (RSGs). During the LBV and RSG stages, stellar mass loss strips off the hydrogen-rich envelope to expose the helium-rich layer, and the star enters the WR phase.

Owing to its high luminosity, massive stars lose mass throughout their lifetime. During the main sequence, O stars have fast stellar winds; during the LBV or RSG phase, a dense slow wind develops; and during the WR phase, a dense fast stellar wind emerges. The velocities and mass loss rates of these winds are shown in the chart in Figure 1.

As a massive star evolves through different phases, its mass loss interacts with the ambient medium that has been modified by the previous mass loss. It is conceivable that a main-sequence O stars fast stellar wind will sweep up the ambient interstellar medium (ISM) into an interstellar bubble [3,4], the slow winds of LBVs and RSGs form circumstellar nebulae in the bubble interiors, and finally the WR wind sweeps up the circumstellar material to form a circumstellar bubble inside the interstellar bubble. An example of such nested bubbles, NGC6164-5, is shown in the left panel of Figure 2.

The formation of planetary nebulae (PNe) is very similar to the formation of circumstellar bubbles of WR stars. As a low- or intermediate-mass star evolves into a red giant or asymptotic giant branch (AGB) star, the copious mass loss forms a circumstellar nebula, and during the subsequent evolution toward white dwarf, a fast stellar wind develops and sweeps up the circumstellar nebula to form a PN [5,6]. The right panel of Figure 2 shows a PN, where the bright main shell consists of the swept-up AGB wind and the surrounding envelope unperturbed AGB wind.

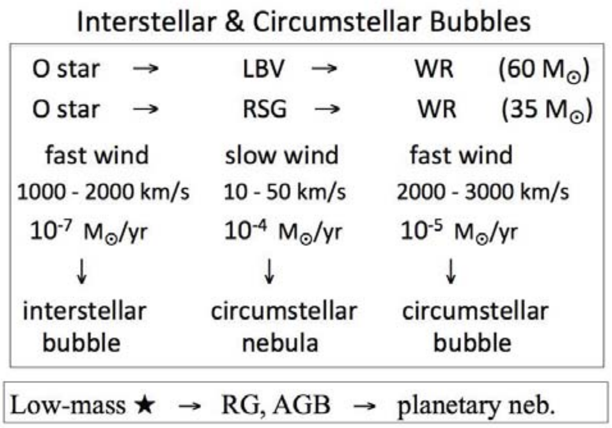

Figure 1. Stellar mass loss at different stages of stellar evolution. Stellar wind velocity and mass loss rates are listed.

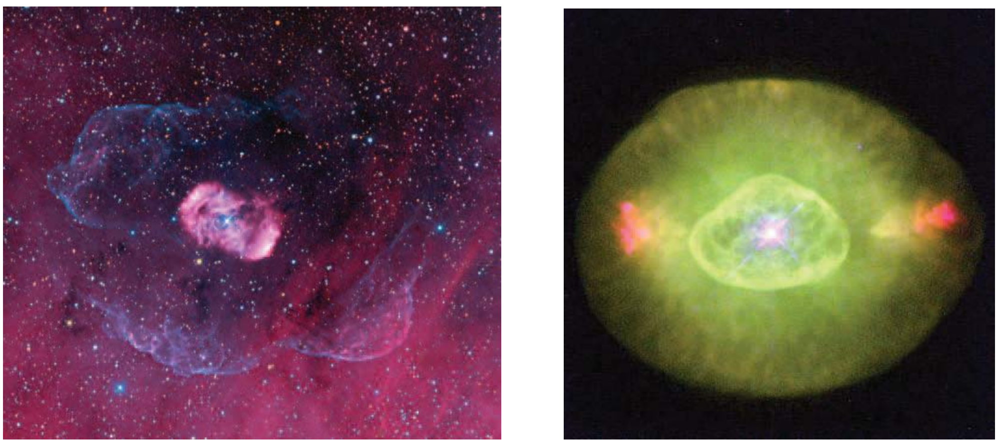

Figure 2. Left: Ground-based image of NGC 6164-5. The small (2 pc ×3 pc) nebula around the central star is a circumstellar bubble consisting of ejected stellar material, while the large (10 pc ×15 pc) shell is the interstellar bubble consisting of interstellar material. The central star is of spectral type O6.5f?p, not yet a WR star. Image credit: Don Goldman. Right: Hubble Space Telescope WFPC2 image of NGC 6826. The bright inner shell is a bubble consisting of swept-up AGB wind, while the envelope contains uninterrupted expanding AGB wind.

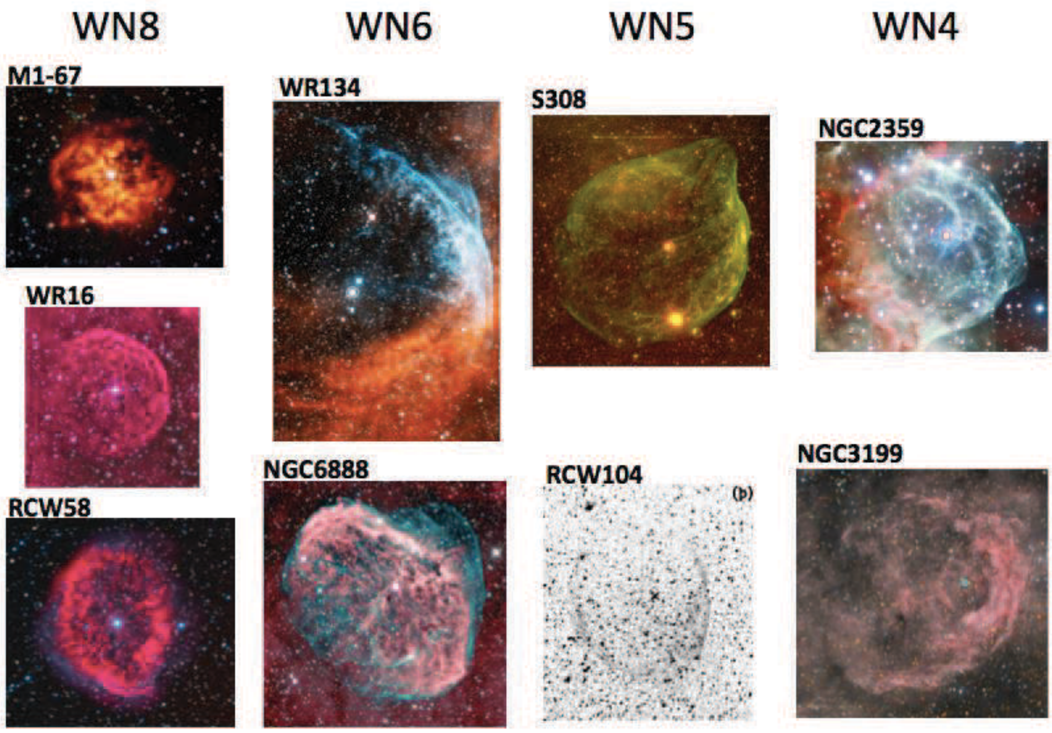

Figure 3. Images of WR nebulae. The spectral types of the central WR stars are marked above each column. Image credits: Hubble Space Telescope (M1-67), Don Goldman (WR16, RCW58), Bob Franke (NGC6888), Travis Rector (WR134), Robert Gruendl and You-Hua Chu (S308, RCW104), ESO/VLT (NGC2359), Velimir Popov and Emil Ivanov (NGC3199).

2. Observed morphologies of WR nebulae

Owing to the high qualities of affordable telescopes/CCD cameras/filters, amateur astronomers have been taking the best images of WR nebulae and made them available on the web. Figure 3 shows 9 Galactic WR nebulae associated with WR stars of different subtypes. There is an apparent correlation between the nebular morphology and the spectral type.

Most WR nebulae are associated with WN stars. The nebulae associate with late-type WN8 stars are dominated by stellar ejecta [7], and have the clumpiest morphology. Despite the large surface brightness fluctuations, the expansions of these nebulae are quite regular [8,9]. In contrast, the nebulae associated with early-type WN4 stars consist of mostly interstellar material [7,10]. The intermediate WN stars, WN5-6, show circumstellar bubble with various degrees of ablation by the fast WR winds.

The morphologies of WR nebulae have been satisfactorily reproduced by hydrodynamic models of nebular evolution from main sequence O to WR stages, taking into account of the mass loss history [11,12,33,34,35,36]. The clumpy morphology of circumstellar bubbles is caused by instability in the shell when the circumstellar material (the slow wind from the LBV or RSG phase) has been swept up.

An intriguing puzzle is that the interstellar bubble blown by a WR stars main-sequence progenitor is rarely observed. In fact, main-sequence O stars are hardly ever seen in interstellar bubbles, despite theoretical expectations [3,4]. To solve this puzzle, Hubble Space Telescope images of the H II region N11B around the OB association LH10 were obtained. LH10 still contains O3V stars, the most massive main sequence stars, indicating that this OB association has not had any supernova explosion yet, and the presence of dense ionized gas in N11B should allow O stars to blow interstellar bubbles. The Hubble images do not show any ring-like morphological features corresponding to bubbles; however, long-slit echelle spectrograms of the [N II] λ6583 line (Figure 4) do show line splitting indicating the existence of expanding shells of sizes $\sim$ 15 pc and expansion velocities $15 - 20$ km s^{-1} [13]. For such low expansion velocities, line-split cannot be seen in the Hα line because of its large thermal width, $\sim$ 20 km s^{-1}, so they have escaped detection in the past. The absence of visible ring-like morphological features in Hα image is also caused by the low expansion velocity: for the 10 km s^{-1} sound velocity of a 10^4 K H II region, the expansion of the bubble is associated with very weak shocks, with Mach number of $1.5 - 2$. Such weak shocks do not produce strong compression of the ISM to produce a density jump for a visible limb-brightened shell nebula. The puzzle is solved.

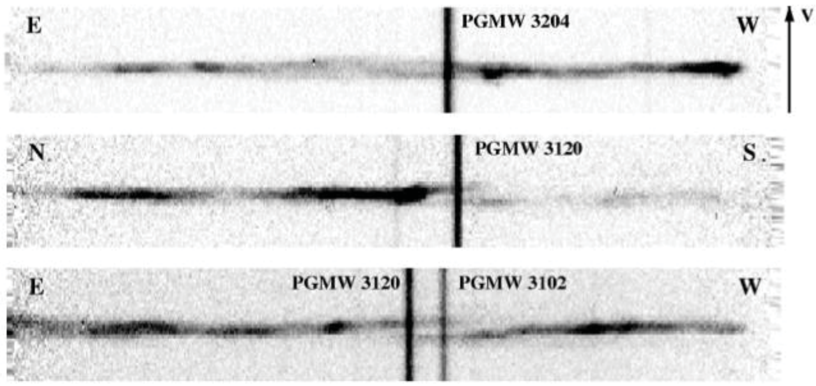

Figure 4. Three long-slit echelle spectrogram of [N II] λ6583 line centered on O stars in LH10/N11B. The horizontal axis is along the slit and the vertical axis is along the dispersion. The star names are marked next to the stellar continua.

3. Extragalactic WR nebulae

WR nebulae have been surveyed in the Large and Small Magellanic Clouds (LMC and SMC) [14,15]. Recent Hα survey of the LMC made with the CTIO Blanco 4m telescope and the MOSAIC camera has been used to study WR nebulae (in preparation). The examples displayed in Figure 5 show significantly more details than previous images taken with Curtis Schmidt Telescope. Some WR nebulae seem to be attached to the inner rims of superbubbles. Often the WR nebulae are best seen in the [O III] λ5007 line because they have higher excitation than the background H II region, for example, the WR bubble around Br12 in DEM L45 (Figure 5). From the surveys of the WR nebulae in the LMC and SMC, we have learned that the large shell structures around WR stars identified in low-resolution images are mostly superbubbles with sizes greater than $\sim$ 100 pc [14], and that high-resolution images are needed to reveal small circumstellar bubbles of WR stars.

Surveys of WR nebulae have been extended to M31 and M33 in the Local Group [16,17]. The ground-based images used in these surveys are of relatively low resolution. While many small WR nebulae (smaller than $\sim$ 40 pc in diameter) are identified as candidates of WR bubbles, their structures are not well resolved; furthermore, a significant fraction of the WR nebulae identified are actually superbubbles around OB associations.

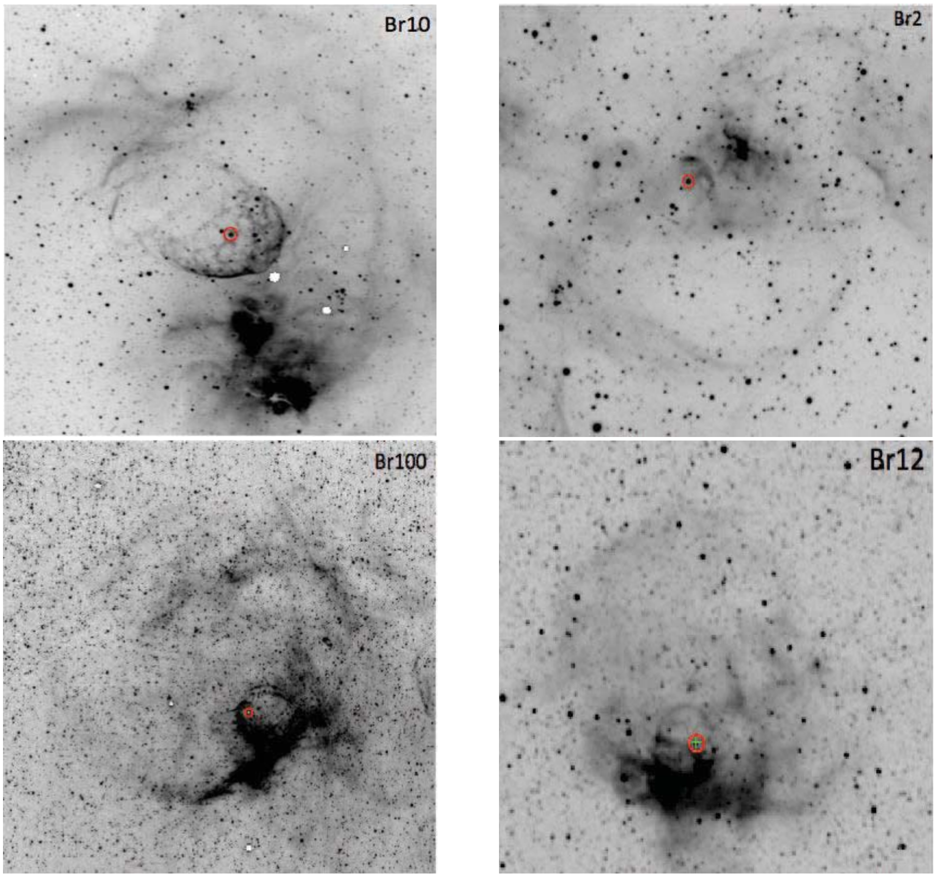

Figure 5. Images of WR nebulae in the LMC. The Hα images of Br2, Br10, and Br100 were taken with the CTIO 4m MOSAIC camera. The MCELS [O III] λ5007 image of Br12 was taken with the Curtis Schmidt Telescope.

4. He II-emitting WR nebulae
Unlike PNe, H II regions photoionized by main-sequence massive stars do not emit He II recombination lines because O stars do not have temperatures much higher than $\sim 50,000$ K; however, some He II regions ionized by WR stars exhibit He II λ4686 line emission, indicating that He is doubly ionized and that the stellar effective temperatures are as high as $85,000 - 100,000$ K. Examples include G2.4 + 1.4 around the WO star WR102 in the Galaxy [18], N79 around the WN2 star Br2 in the LMC, and N76 around the WN2 star AB7 in the SMC [19]. See Figure 6.

5. Hot gas in WR nebulae
Circumstellar bubbles of WR stars are ideal laboratories to study a number of astrophysical problems: hydrodynamic interactions between fast stellar winds and circumstellar material, stellar wind energy feedback, and thermal conduction between hot gas and cool gas. The bubble interior filled by shocked fast wind is expected to emit in X-rays, while the conduction layer between the hot interior gas and the cool bubble shell gas contains highly ionized species produced by thermal collisions, and is best studied in ultraviolet wavelengths. Multi-wavelength observations are needed to obtain thorough understandings of WR bubbles.

X-ray emission from the hot gas in bubble interiors is first detected in the WR nebula NGC

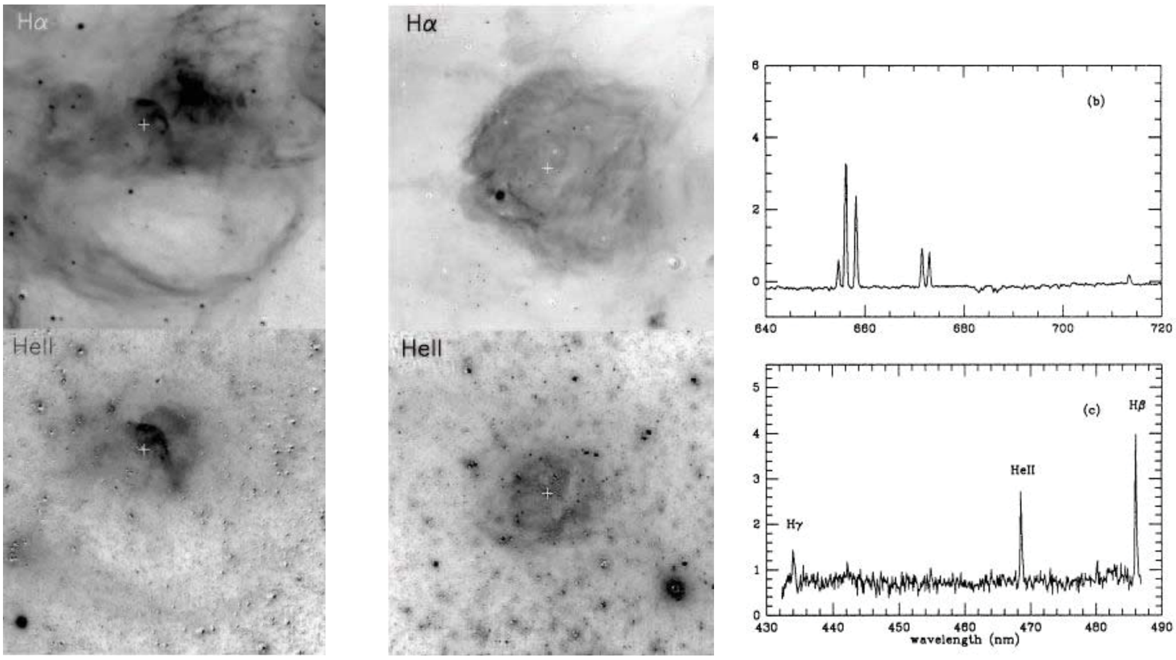

Figure 6. Left - Hα and He II λ4686 images of Br2 in the LMC [19]. Middle - Hα and He II λ4686 images of AB7 in the SMC [19]. Right - optical spectrum of G2.4 + 1.4 around WR102 in the Galaxy [18].

6888 using Einstein Observatory data [20]. ROSAT observations of the WR bubble S308 show hint of diffuse X-ray emission [21]. XMM-Newton observations of S308 confirmed the diffuse X-ray emission and produced its first useful X-ray spectrum; furthermore, XMM-Newton mapped S308 and presented a complete X-ray view of S308 [22,23]. Recently, XMM-Newton observations detected faint diffuse X-ray emission from the interior of WR bubble NGC 2359 [24,25]. The X-ray spectra of these three WR bubbles are very soft, and thermal plasma emission model fits indicate that the hot gas temperatures are only $1 - 2 \times 10^6$ K (Figure 7) [26]. As the emission measure is proportional to the density squared, the diffuse X-ray emission from a bubble interior should peak near the conduction layer where the density is high and temperature is low, qualitatively in agreement with the plasma temperatures implied by the X-ray spectra. However, hydrodynamic models of bubbles taking into account of thermal conduction, dynamic mixing, and radiative cooling have not been able to reproduce the very soft spectra of diffuse X-ray emission from WR bubbles [27].

Thermal conduction layers in bubbles or superbubbles had been studied with C IV and Si IV absorption lines, but the early investigations using International UV Explorer (IUE) observations of early-type stars yielded ambiguous results because C^{3+} and Si^{3+} can be produced by photoionization. The first unambiguous detection of conduction layer was provided by HST GHRS observations of the N V absorption line against the spectrum of HD50896, the central WR star of S308 [28]. Attempts to use HST STIS observations to detect N V λλ1238,1242 lines in emission from the interface layer of S308 has not been successful.

PNe have much higher density than WR bubbles, so their interface layers can be more easily detected. For example, O VI λλ1031,1037 lines and N V λλ1238,1242 lines have been detected both in emission (off the central star) and absorption (against the stellar spectra) in the Cat's Eye PN, NGC 6543 [29,30].

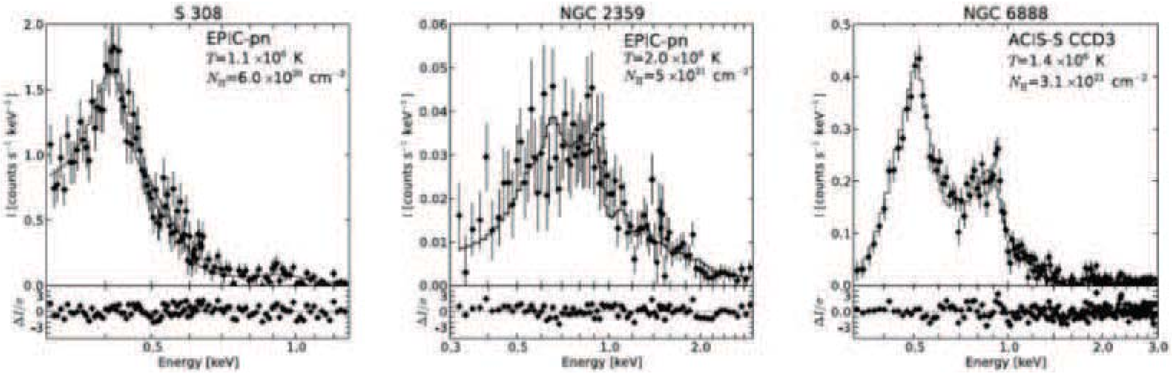

Figure 7. X-ray spectra of the hot gas in the WR bubbles S308, NGC2359, and NGC6888. The X-ray observations of S308 and NGC2359 were made with the XMM-Newton X-ray Observatory, and the X-ray observation of NGC6888 was made with the Chandra X-ray Observatory. This figure is taken from [26].

6. Stellar evolution constrained by WR nebular abundances

Circumstellar bubbles of WR stars contain material ejected by the progenitors. Depending on the previous evolutionary paths, whether through LBV or RSG, the stellar ejecta consist of processed stellar material whose elemental abundance reflects the nature of the WR stars' progenitors [7]. It is difficult to determine elemental abundances of WR bubbles because they are more often than not superposed on bright H II regions, and the background H II region contamination needs high-resolution spectra to identify and remove it. Figure 8 shows high-dispersion spectra of RCW58 and NGC6888; it can be seen that the background H II region has a nearly constant velocity throughout the slit length and the approaching and receding sides of the WR bubble appear blue- and red-shifted from the H II region component, respectively [9]. It is interesting to note that despite the large surface brightness variations, the expansion of the WR bubble is quite regular.

High-dispersion spectra covering all essential nebular lines have been obtained and analyzed for abundance only for the WR bubble NGC6888 [31,32]. These studies investigated trace of the CNO cycle and determined that the progenitor of the WR star in NGC6888 had an initial mass between 25 and $40M_{\odot}$. Advances in modern instrumentation have made it possible to obtain high-dispersion spectra for large wavelength ranges (e.g. $3700 - 7400$ Å, the High-Dispersion Spectrograph of the Subaru Telescope) so that bubble and background H II region components can be resolved and analyzed separately. Future observations should be made systematically for WR bubbles of different spectra types and physical properties, so that their abundances can be compared with those expected from models of stellar evolution. WR bubbles from galaxies of different metallicities should also be studied to see how metallicity affects stellar evolution.

References

[1] Johnson H M and Hogg D E 1965 *Astrophs. J.* **142** 1033
[2] Humphreys R M and Davidson K 1979 *Astrophys. J.* **232** 409
[3] Castor J, McCray R and Weaver R 1975 *Astrophys. J.* **200** L107
[4] Weaver R, McCray R, Castor J, Shapito P and Moore R 1977 *Astrophys. J.* **218** 377
[5] Kwok S 1983 *Planetary Nebulae* ed Flower D R (Proc. Int. Astron. Union S103) 293
[6] Frank A, Balick B and Riley J 1990 *Astron. J.* **100** 1903
[7] Esteban C, Vílchez J M, Smith L J and Clegg R E S 1992 *Astron. Astrophys.* **259** 629
[8] Solf J and Carsenty U 1982 *Astron. Astrophys.* **116** 54
[9] Chu Y-H 1988 *Pub. Astronom. Soc. Pac.* **100** 986
[10] Esteban C, Vílchez J M, Manchado A and Edmunds M G 1990 *Astron. Astrophys.* **227** 515

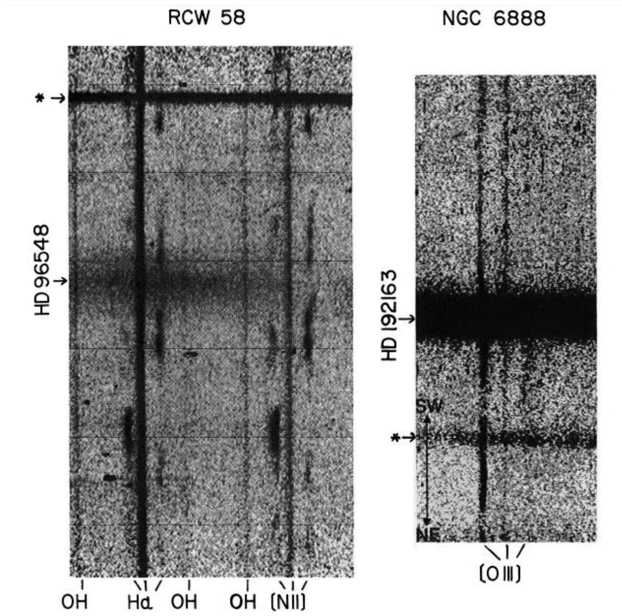

Figure 8. Long-slit high-dispersion echelle spectra of RCW58 and NGC6888. The spectral dispersion is along the X-axis and the spatial direction is along the Y-axis. This figure is reproduced from [9].

[11] García-Segura G, Langer N and Mac Low M-M 1996 *Astron. Astrophys.* **316** 133
[12] García-Segura G, Mac Low M-M and Langer N 1996 *Astron. Astrophys.* **305** 229
[13] Nazé Y, Chu Y-H, Points S D, Danforth C W, Rosado M and Chen C-H R 2001 *Astronom. J.* **122** 921
[14] Chu Y-H and Lasker B 1980 *Pub. Astron. Soc. Pac.* **92** 730
[15] Dopita M A, Bell J F, Chu Y-H and Lozinskaya T A 1994 *Astrophys. J. Suppl. Series* **93** 455
[16] Bransford M A, Thilker D A, Walterbos R A M and King N L 1999 *Astronom. J.* **118** 1635
[17] Drissen L, Shara, M M and Moffat A F J 1991 *Astronom. J.* **101** 1659
[18] Polcaro V F, Rossi C, Norci L and Viotti R 1995 *Astron. Astrophys.* **303** 211
[19] Nazé Y, Rauw G, Manfroid J, Chu Y-H and Vreux J-M 2003 *Astron. Astrophys.* **408** 171
[20] Bochkarev N G 1988 *Nature* **332** 518
[21] Wrigge M 1999 *Astron. Astrophys.* **343** 599
[22] Chu Y-H, Guerrero M A, Gruendl R A, Garcia-Segura G and Wendker H J 2003 *Astrophys. J.* **599** 1189
[23] Toalá J A, Guerrero M A, Chu Y-H, Gruendl R A, Arthur S J, Smith R C and Snowden S L 2012 *Astrophys. J.* **755** 77
[24] Zhekov S A 2014 *Mon. Not. R. Astronom. Soc.* **443** 12
[25] Toalá J A, Guerrero M A, Chu Y-H and Gruendl R A 2015 *Mon. Not. R. Astron. Soc.* **446** 1083
[26] Toalá J A, Guerrero M A, Chu Y-H, Arthur S J and Gruendl R A 2015 *Wolf-Rayet Stars: Proceedings of an International Workshop* eds Hamann W-R, Sander A and Todt H p 333
[27] Toalá J A and Arthur S J 2014 *Mon. Not. R. Astron. Soc.* **443** 3486
[28] Boroson B, McCray R, Clark O, Slavin J, Mac Low M-M, Chu Y-H and Van Buren D 1997 *Astrophys. J.* **478** 638
[29] Gruendl R A, Chu Y-H and Guerrero M A 2004 *Astrophys. J.* **617** L127
[30] Fang X, Guerrero M A, Toalá J A, Chu, Y-H and Gruendl R A 2016 *Astrophys. J.* **822** L1
[31] Esteban C and Vílchez J M 1992 *Astrophys. J.* **390** 536
[32] Mesa-Delgado A, Esteban C, García-Rojas J, Reyes-Pérez J, Morisset C and Bresolin F 2014 *Astrophys. J.* **785** 100
[33] Freyer T, Hensler G and Yorke H W 2003 *Astrophys. J.* **594** 888
[34] Freyer T, Hensler G and Yorke H W 2006 *Astrophys. J.* **638** 262
[35] Toalá J A and Arthur S J 2011 *Astrophys. J.* **737** 100
[36] van Marle A J and Keppens R 2012 *Astron. Astrophys.* **547** A3